# Dependence of nonlinearity enhancement on power density in photonic crystals characterized by numerical *Z*-scan experiments based on the finite-difference time-domain technique

**Zi-Ming Meng,[1] Hai-Ying Liu,[1] Qiao-Feng Dai,[1] Li-Jun Wu,[1] Qi Guo,[1] Wei Hu,[1] Song-Hao Liu,[1] Sheng Lan,[1,*] and V. A. Trofimov[2]**

[1]*Laboratory of Photonic Information Technology, School for Information and Optoelectronic Science and Engineering, South China Normal University, Guangzhou 510006, Guangdong, China*
[2]*Department of Computational Mathematics and Cybenetics, M. V. Lomonosov Moscow State University, Moscow 119992, Russia*
[*]*Corresponding author: slan@scnu.edu.cn*

Received December 7, 2007; accepted January 14, 2008;
posted February 13, 2008 (Doc. ID 90644); published March 21, 2008

We investigate the enhancement of nonlinearity in one-dimensional (1D) photonic crystals (PCs) with Kerr nonlinearity by numerical *Z*-scan experiments based on the finite-difference time-domain technique. Focused Gaussian beams with well-defined waists and Rayleigh lengths necessary for *Z*-scan experiments are generated through a conjugated manipulation of the Gaussian beams propagating in free space. The *Z*-scan measurements used for bulk materials are naturally extended to 1D PCs after incorporating the frequency- and power-density-dependent reflections into their linear and nonlinear absorptions. The closed- and open-aperture *Z*-scan traces for the 1D PCs are obtained and a symmetric method is employed to modify the asymmetric closed-aperture traces. The nonlinearity enhancement factors at different frequencies in the first and second bands are derived numerically and analytically. A good agreement is found between the numerical and analytical results in the case of weak nonlinearity. Moreover, the dependences of the enhancement factor on the incident power density for different frequencies in the 1D PCs are extracted and they are found to be much different from those in bulk materials. It is revealed that the variation of the group velocity with increasing power density is responsible for the power-density dependence of the enhancement factor. It indicates that in practice one must deliberately choose the working frequency and power density of PC-based devices in order to achieve a maximum enhancement of nonlinearity. 

*OCIS codes:* 190.3270, 190.4390.

## 1. INTRODUCTION

Since the pioneer works of Yablonovitch [1] and John in 1987 [1,2], the physical properties of photonic crystals (PCs) have been widely explored for the construction of sophisticated devices with various functions. At the beginning, most investigations were focused on passive devices such as cavities [3], filters [4,5], waveguides [6], delay lines [7,8], superprisms [9], and collimators [10,11] among others. In recent years, attention has been shifted to active devices constructed with nonlinear PCs such as optical limiters [12,13], switches [14–18], diodes [19], and so on. It is expected that the interaction between light and material can be significantly enhanced due to the slow light effect occurring at the band edges of PCs. Accordingly, much effort has been devoted to the study of the nonlinearity enhancement in nonlinear PCs. A simple analysis of the phase shift achieved in a nonlinear PC waveguide gives an enhancement factor that is inversely proportional to the square of the group velocity in the PC waveguide [20]. Sometimes it is convenient to use the density of modes (DOM) to describe the enhancement effect. Thus, it implies that the enhancement of nonlinearity is proportional to the square of the DOM.

Although the relationship between the enhancement factor and the group velocity (or DOM) is quite important in the design of PC-based devices, a direct verification of it is still lacking. Several years ago, Haché and Bourgeois [17] carried out *Z*-scan measurements for a one-dimensional (1D) $Si/SiO_2$ PC and derived the effective nonlinear coefficient. However, they focused mainly on the switching behavior of the 1D PC and did not discuss the nonlinearity enhancement factor. After that, Hwang *et al.* [21] and Hwang and Wu [22] performed nonlinear transmission and *Z*-scan measurements for cholesteric liquid crystals, which possess 1D photonic bandgaps. The nonlinearity enhancement factor was extracted and compared with the DOM calculated theoretically. However, the discrepancy was quite large because of the complexity of cholesteric liquid crystals. It is noticed that they proposed to use an intensity-dependent wave vector to characterize the change in the refractive index and transmission (or reflection) induced by the nonlinear response of the PCs. Actually, the enhancement of nonlinearity originates from the two features of PCs. One is the well-known slow light effect and another is the shift of the photonic bands, which is inevitable in nonlinear PCs. In the linear

 

case, one can accurately define the group velocity at a certain frequency. When nonlinearity is concerned, however, the situation is complicated by the shift of photonic bands induced by the nonlinear refractive index change. In this case, we expect that both the group velocity and the DOM at a certain frequency become dependent on the power density of the incident wave. Therefore, the relationship given above is applicable only in the cases of weak nonlinearity and the enhancement factor should exhibit a strong dependence on the power density of the incident wave when the weak nonlinearity condition is not satisfied.

In practice, the *Z*-scan technique has become an effective method to characterize the nonlinear coefficients of physically thin films, including both the real and imaginary parts [23]. It has been employed to study the enhancement of nonlinearity in 1D PCs [22,24]. However, a numerical *Z*-scan experiment based on the finite-difference time-domain (FDTD) technique has not yet been established. The key point of using the FDTD technique in numerical *Z*-scan experiments is the generation of focused Gaussian beams with well-defined waists and Rayleigh lengths. Also, the application of such a *Z*-scan experiment on nonlinear 1D PCs needs to be investigated in detail.

In this paper, we present a detailed study on the enhancement of nonlinearity in 1D PCs by utilizing numerical *Z*-scan experiments established by the FDTD technique [25]. It is revealed that the enhancement factor exhibits a strong dependence on the incident power density. In the limit of weak nonlinearity, it is inversely proportional to the square of the group velocity. In addition, we have established an effective method in which the frequency- and power-density-dependent reflections in PCs are well incorporated into the linear and nonlinear absorptions and the asymmetric closed-aperture traces are made to be symmetric. Also, we explain the physical origin for the abnormal *Z*-scan traces observed at the valleys of the transmission spectra. The paper is organized as follows. In Section 2, we describe the structure of the 1D PC used in our study and the generation of focused Gaussian beams with well-defined waists and Rayleigh lengths. In Section 3, we discuss how to accommodate the frequency- and power-density-dependent reflections in order to extend the *Z*-scan experiments from bulk materials to nonlinear PCs and how to modify the obtained asymmetric *Z*-scan traces by using a symmetric method. In Section 4, we present the results of the numerical *Z*-scan experiments for the 1D PC and derive the nonlinearity enhancement factors with respect to the bulk material for different frequencies. Then, an analytical expression for the enhancement factor is derived and a comparison between the numerical and analytical results is made in Section 5. In Section 6, the power-density dependences of the enhancement factor at different frequencies are presented and the physical origin is discussed. Finally, a summary of our research is given in Section 7.

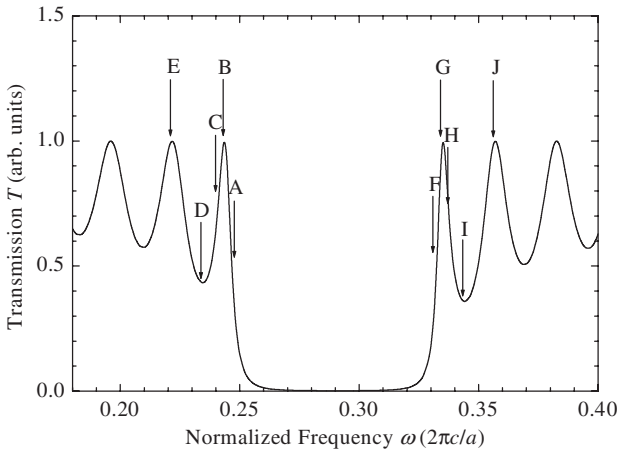


Fig. 1. (Color online) Linear transmission spectrum for the 1D PC studied in this paper. The frequencies at which the enhancement of nonlinearity is investigated are indicated by arrows.

## 2. STRUCTURE OF THE 1D PHOTONIC CRYSTAL AND GENERATION OF FOCUSED GAUSSIAN BEAMS

The 1D PC used in our study consists of 10 periods of a bilayer structure. The linear refractive indices of the two constituent materials of the bilayer structure are chosen to be $n_{10}=1.45$ and $n_{20}=2.14$, which correspond to the refractive indices of $SiO_2$ and $TiO_2$, respectively, at 500 nm [26]. Their thicknesses are set to be $d_1=0.3\ \mu$m and $d_2=0.2\ \mu$m. Thus, the period and total length of the 1D PC are $d=0.5\ \mu$m and $L^{PC}=5\ \mu$m. The thin film condition required in *Z*-scan measurements is satisfied, as will be shown later. In our study, we consider only the third-order nonlinearity in the $TiO_2$ layer while that in the $SiO_2$ layer is neglected. The nonlinear coefficient for the $TiO_2$ layer is chosen to be $n_2=1\times10^{-4}\ \mu m^2/W$ (or $1\times10^{-12}\ cm^2/W$) in the numerical simulations. Also, it is assumed that both materials work in the transparent region where the absorption is negligible. As will be shown in Section 3, the frequency- and the power-density-dependent reflections can be included in the linear and nonlinear absorptions of the 1D PC.

The linear transmission spectrum of the 1D PC obtained by the FDTD simulation is shown in Fig. 1. A sufficiently small incident power density is used in the simulation in order to avoid any shift of the photonic bands. In the FDTD simulations, the grid sizes along the $x$ and $z$ directions are chosen to be 0.2 and 0.05 $\mu$m and a perfectly matched layer boundary condition is employed. On the linear transmission spectrum, we have used arrows to mark the frequencies at which the enhancement of nonlinearity is going to be investigated by the numerical *Z*-scan experiments. Since a large enhancement of nonlinearity is anticipated for the frequencies near the band edges, we choose to study the high-frequency side of the first band and the low-frequency side of the second band. Particularly, our attention is paid to those frequencies where the transmission peaks or valleys appear.

It is apparent that the key procedure to implement a numerical *Z*-scan experiment by using the FDTD technique is the generation of focused Gaussian beams with well-defined waists and Rayleigh lengths. To do so, we have employed a conjugated technique to generate focused Gaussian beams from the data of the Gaussian beams propagating in free space. To minimize the differ-

ence in Rayleigh length for different frequencies, we fix the waist of the Gaussian beam at the focus to be 4 $\mu$m. After propagating in free space for a sufficiently long time, the data of the Gaussian beam is extracted at the boundary of the simulation area that is surrounded by perfectly matched layers. Then, the wavefront of the focused Gaussian beam can be obtained through a conjugated manipulation of the data. Once we send the data back into our simulation area as an excitation profile, a focused Gaussian beam with well-defined waist and Rayleigh length appears.

The electric field distribution of a focused Gaussian beam generated by using the above method is shown in Fig. 2. For closed-aperture measurements, a tiny power detector of 0.2 $\mu$m is placed at the position of $z=58$ $\mu$m. This arrangement satisfies the far-field condition required for the $Z$-scan experiments. As for open-aperture measurements, a power detector of sufficiently wide is put at the position of $z=34$ $\mu$m. In all simulations, the 1D PC is moved along the $z$ axis from $z=-30$ to 30 $\mu$m with a step of 2 $\mu$m. The scanning range is approximately equal to five times the Rayleigh length.

## 3. EFFECT OF PHOTONIC BAND SHIFT IN *Z*-SCAN EXPERIMENTS

For bulk materials in which Kerr nonlinearity and two-photon absorption are present simultaneously, the dependence of the refractive index on light intensity can be expressed as

$$n(I) = n_0 + n_2 I, \tag{1}$$

where $n_0$ is the linear refractive index, $n_2$ is the nonlinear coefficient, and $I$ is light intensity. Similarly, the dependence of the absorption on light intensity can be described as

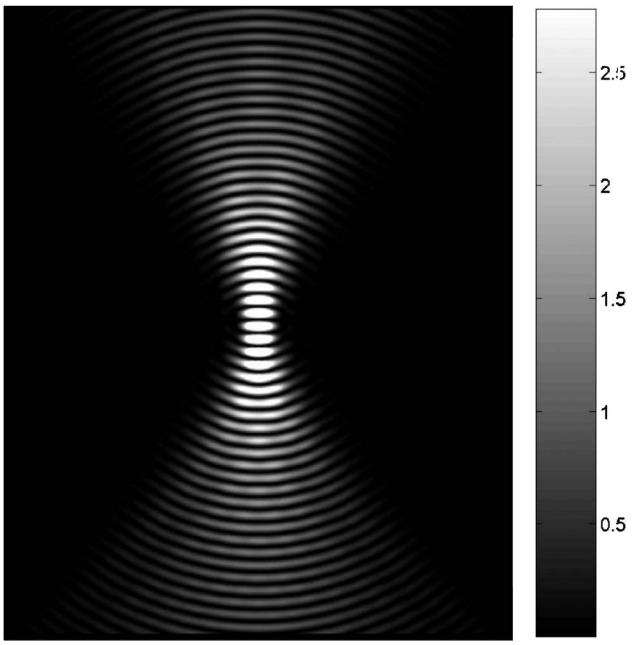


Fig. 2. (Color online) Electric field distribution of the focused Gaussian beams generated by a conjugated technique.

$$\alpha(I) = \alpha_0 + \beta I, \tag{2}$$

where $\alpha_0$ and $\beta$ are the linear and nonlinear absorption coefficients, respectively.

In general, the values of $n_2$ and $\beta$ can be easily determined by performing $Z$-scan measurements on thin films in the closed- and open-aperture forms. For PCs, the situation is different even in the linear case. Even though the PCs are composed of lossless materials, the intrinsic multiple reflections result in a frequency-dependent reflection. When nonlinearity is concerned, the situation is more complicated because the change of refractive index generally leads to the shift of the photonic bands. In our case, the photonic bands are moved towards the low-frequency side if the nonlinear coefficient $n_2$ is positive. Since the reflection and transmission of PCs are frequency dependent, the shift of the photonic bands will result in a change in the reflection or transmission that is dependent on the power density. These two features of nonlinear PCs will significantly influence the results of $Z$-scan experiments and their explanations. Therefore, whether we can extend the $Z$-scan experiments from bulk materials to PCs is determined by whether we can treat the two features properly and reasonably. Fortunately, a careful examination suggests that we can include the frequency- and the power-density-dependent reflections into the linear and nonlinear absorptions of PCs. Consequently, nonlinear PCs composed of lossless materials are considered to be absorptive. Their absorption coefficients can be written as

$$\alpha(\omega, I) = \alpha_0(\omega) + \beta(\omega) I, \tag{3}$$

where $\alpha_0(\omega)$ and $\beta(\omega)$ represent the equivalent linear and nonlinear absorption coefficients. This treatment is proved to be reasonable by the simulated open-aperture traces given in Section 4. It is remarkable that both the linear and nonlinear absorption coefficients are frequency dependent.

Having incorporated the linear and nonlinear reflections of PCs into the linear and nonlinear absorptions, we can extend the $Z$-scan experiments used for bulk materials to nonlinear PCs, including the theoretical analysis and the explanation of the experimental results. Under the condition of small phase distortion and small aperture, the on-axis phase shift is proportional to the peak-to-valley transmission difference in the closed-aperture trace [23], i.e.,

$$\Delta\phi_0 \propto \Delta T_{p-v}. \tag{4}$$

For bulk materials, it is easy to derive that

$$\Delta\phi_0 = k n_2 I_0 L_{\text{eff}}^{\text{bulk}}, \tag{5}$$

where $k$ is the wave vector, $I_0$ is the light intensity, and $L_{\text{eff}}^{\text{bulk}} = (1 - e^{-\alpha_0 L^{\text{bulk}}})/\alpha_0$ is the effective length. Here, $\alpha_0$ is the linear absorption coefficient of the bulk material. Therefore, the nonlinear coefficient $n_2$ can be easily deduced from $\Delta T_{p-v}$. For PCs, we can accordingly define the effective length as $L_{\text{eff}}^{\text{PC}}(\omega) = (1 - e^{-\alpha_0(\omega) L^{\text{PC}}})/\alpha_0(\omega)$. Thus, the effect of linear absorption (or reflection) will be manifested in the reduction of $L_{\text{eff}}^{\text{PC}}$. Similarly, the value of $\Delta T_{p-v}$ will reflect the effective nonlinear coefficient, which

is generally different from the nonlinear coefficients of the constituent materials.

To test the effectiveness of the numerical $Z$-scan experiments based on the FDTD technique, we first carried out closed- and open-aperture $Z$-scan measurements on a bulk material, which is a $TiO_2$ film of 2 $\mu$m. In the following, this sample is used as a reference for characterizing the nonlinearity enhancement factor. The normalized $Z$-scan trace for the $TiO_2$ film obtained by a division method is shown in Fig. 3(a) by filled circles. It is similar to the standard $Z$-scan traces of bulk materials except the symmetric axis in the vertical direction is slightly above $T=1$ [23]. It can be attributed to the small reflection of the $TiO_2$ film. In comparison, we also performed $Z$-scan measurements for the 1D PC and derived the normalized $Z$-scan trace at a frequency of $\omega_G$, as shown in Fig. 3(b). Compared with the standard $Z$-scan traces of bulk materials, it is found that the $Z$-scan trace of the PC is not symmetric with respect to $z=0$ and $T=1$.The physical origin for this asymmetry has been ascribed to the large nonlinear absorption (i.e., the large reflection) in the PC [27]. Fortunately, it has been demonstrated that the error in determining $\Delta\phi_0$ and $n_2$ caused by this asymmetry can be minimized by using a symmetric method [27]. A detailed description of the method can be found in [27]. The rectified $Z$-scan traces obtained by adopting this method are also shown in Fig. 3 for comparison. It is obvious that the rectified traces become symmetric with respect to $z=0$ and $T=1$. Hence, the value of $\Delta T_{p-v}$ that reflects the effective nonlinear coefficient of the PC can be accurately extracted. In the following, all of the $Z$-scan traces are obtained in this way.

## 4. RESULTS OF NUMERICAL $Z$-SCAN EXPERIMENTS

The rectified closed- and open-aperture $Z$-scan traces obtained for the 1D PC at different frequencies are presented in Figs. 4 and 5, respectively. In all simulations, the power density of the incident wave is fixed to be $1 \times 10^2$ W/$\mu$m. From the closed-aperture traces, it can be seen that the effective nonlinear coefficient, which is reflected in $\Delta T_{p-v}$, becomes larger when the frequency of the incident wave approaches the band edge. This behavior is the same for the first and second bands, as shown in Figs. 4(a) and 4(b). It is also noticed that the effective nonlinear coefficients in the first band are generally larger than those in the second band. This is easily understood because the field intensity in the first band is concentrated in the $TiO_2$ layer with a larger nonlinearity. One remark-

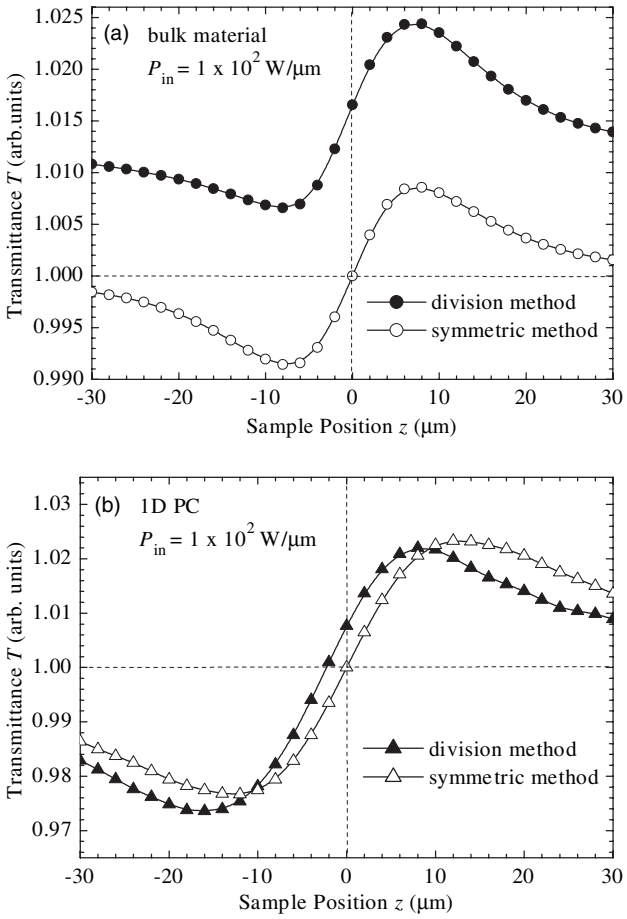


Fig. 3. (Color online) $Z$-scan traces obtained by the division method and the symmetric method for the (a) bulk material ($TiO_2$ film) and (b) 1D PC.

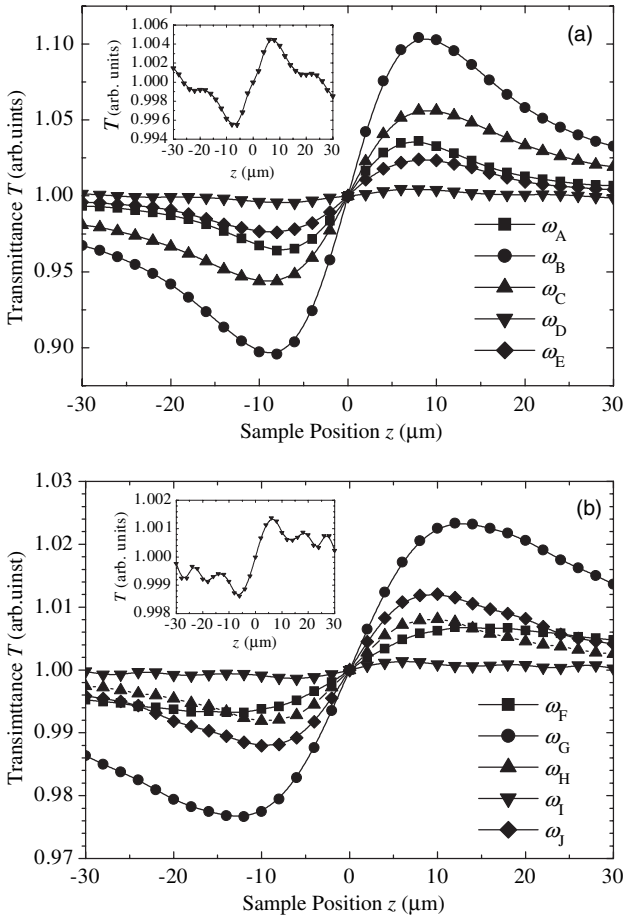


Fig. 4. (Color online) Closed-aperture $Z$-scan traces for the frequencies in the first (a) and (b) second bands. The insets show the details of the $Z$-scan traces obtained at $\omega_D$ and $\omega_I$ where the transmission valleys appear.

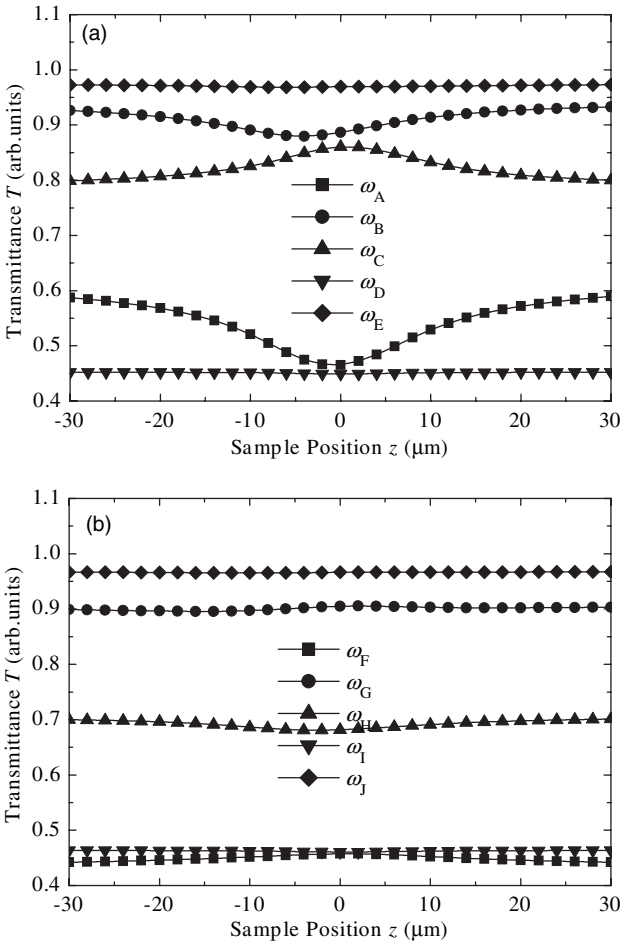


Fig. 5. (Color online) Open-aperture $Z$-scan traces for the frequencies in the (a) first and (b) second bands.

able feature is that the closed-aperture profiles for the frequencies at the transmission valleys are quite strange, as shown in the insets of Figs. 4(a) and 4(b). In this case, the transmittance does not evolve smoothly with the position of the sample, and it affects the determination of $\Delta T_{p-v}$. The physical origin for this behavior will be discussed later in this section. From the open-aperture traces shown in Figs. 5(a) and 5(b), it is remarkable that the change in the transmission or equivalently the reflection is significant for the frequencies near the band edges. It is justified that our treatment of reflection as nonlinear absorption is necessary.

To characterize the enhancement of nonlinearity near the band edges of the 1D PC, we can use the $TiO_2$ film of 2 $\mu$m as a reference and define an enhancement factor $\eta$ as follows:

$$\eta = \frac{\Delta T_{p-v}^{\mathrm{PC}}}{\Delta T_{p-v}^{\mathrm{bulk}}}, \tag{6}$$

where $\Delta T_{p-v}^{\mathrm{PC}}$ and $\Delta T_{p-v}^{\mathrm{bulk}}$ represent the values of $\Delta T_{p-v}$ for the PC and the bulk material. Since $\Delta T_{p-v}^{\mathrm{bulk}}$ does not depend on the frequency, we can take one frequency in the low-frequency side for its $Z$-scan measurements. The enhancement factors for different frequencies in the first and second bands have been derived, and they are presented in Fig. 6.

As mentioned at the beginning, the enhancement of nonlinearity originates partly from the small group velocity near the band edges. In the case of weak nonlinearity, the enhancement factor should be inversely proportional to the square of the group velocity. For the bulk material whose dispersion is neglected, the group velocity is the same as its phase velocity, which is given by $c/n_{20}$, where $c$ is the speed of light in vacuum. On the other hand, the distribution of the group velocity in the 1D PC can be easily calculated by the transfer matrix method. We present the frequency spectra for the transmission, phase, and group velocity in Figs. 7(a)–7(c), respectively. It can be seen that the peaks and valleys in the transmission correspond to the minima and maxima of the group velocity.

From Fig. 7(b), it is noticed that the transmission phase changes from $\pi/2$ to $-\pi/2$ in between the two neighboring transmission valleys. Near the band edges, the separation between the neighboring transmission valleys (or peaks) becomes smaller, implying that the change in the transmission phase becomes steeper. This is more obvious by examining $\mathrm{d}\phi/\mathrm{d}\omega$, which is also plotted in Fig. 7(b). Therefore, the transmission phase change is larger for the frequencies close to the band edges for a fixed band shift. In addition, it can be easily derived that the transmission phase change is inversely proportional to the group velocity, implying that the steep change in the transmission phase near the band edges also contributes a factor of $1/v_g$ to the enhancement factor. Another feature that needs to be addressed is the abrupt change of the transmission phase at the transmission valleys. In $Z$-scan measurements, it is known that the change in the transmittance is related to the phase change induced by nonlinearity at the focus. When the photonic bands are shifted by the nonlinear refractive index change, the abrupt change of the transmission phase at the transmission valleys will lead to the fluctuation in the transmit-

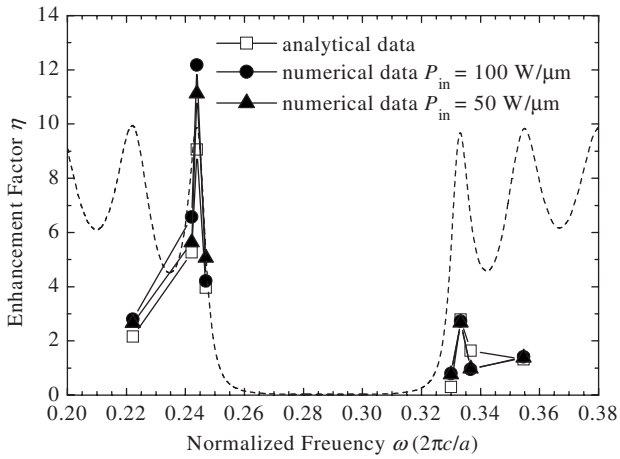


Fig. 6. (Color online) Comparison of the nonlinearity enhancement factors at different frequencies derived numerically (filled circles and triangles) and analytically (open squares). The linear transmission spectrum is also shown by a dashed curve for reference (the transmittance has been multiplied by a factor of 10).

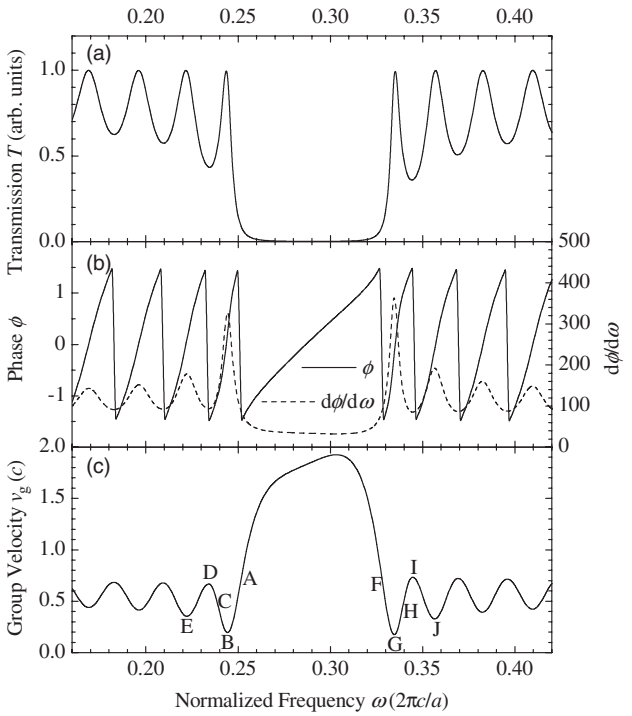


Fig. 7. (Color online) Frequency spectra for (a) transmission, (b) transmission phase and its derivative, and (c) group velocity of the 1D PC calculated by the transfer matrix method.

tance. Therefore, it is responsible for the abnormal closed-aperture profile observed at the transmission valleys.

## 5. NONLINEARITY ENHANCEMENT FACTOR IN PHOTONIC CRYSTALS

It has been clarified that the relationship $\Delta\phi_0 \propto \Delta T_{p-v}$ is applicable for both bulk materials and PCs. Keep in mind that $\Delta\phi_0$ is the on-axis phase shift at the focus; let us see what determines its value. In general, we have [20]

$$\Delta\phi_0 = \delta k L_{\text{eff}}, \tag{7a}$$

$$\delta k \approx \delta\omega\left(\frac{d\omega}{dk}\right)^{-1} = \frac{\delta\omega}{v_g}, \tag{7b}$$

$$\delta\omega = -\sigma\frac{\delta n}{n}\omega. \tag{7c}$$

In Eq. (7c), $\sigma$ specifies the fraction of the total energy of the mode that is stored in the nonlinear medium [20]. Thus, we have $\sigma_{\text{bulk}}=1$ for bulk materials and $0<\sigma_{\text{PC}}<1$ for PCs. In our case, $\sigma$ is frequency dependent and it is large in the first band and small in the second band. Hence, we get

$$\Delta\phi_0 \approx -\sigma\frac{\delta n}{n}\frac{\omega}{v_g}L_{\text{eff}}. \tag{8}$$

On the other hand, $\delta n/n$ is given by [28]

$$\delta n/n = \varepsilon_0 c n_2 |E_0|^2, \tag{9}$$

where $|E_0|^2$ is the electric field intensity at the focus. Therefore, $\Delta\phi_0$ can be written as

$$\Delta\phi_0 \approx -\varepsilon_0 c n_2 |E_0|^2 \frac{\omega}{v_g}\sigma L_{\text{eff}}. \tag{10}$$

Finally, we can derive the expression for the enhancement factor $\eta$ as follows:

$$\eta = \frac{\Delta\phi_0^{\text{PC}}}{\Delta\phi_0^{\text{bulk}}} = \frac{|E_0^{\text{PC}}|^2}{|E_0^{\text{bulk}}|^2}\left(\frac{v_g^{\text{bulk}}}{v_g^{\text{PC}}}\right)\frac{\sigma_{\text{PC}}L_{\text{eff}}^{\text{PC}}}{\sigma_{\text{bulk}}L_{\text{eff}}^{\text{bulk}}} \propto \left(\frac{v_g^{\text{bulk}}}{v_g^{\text{PC}}}\right)^2\frac{\sigma_{\text{PC}}L_{\text{eff}}^{\text{PC}}}{\sigma_{\text{bulk}}L_{\text{eff}}^{\text{bulk}}}. \tag{11}$$

In obtaining the above expression, we have used the relationship between the electric field intensity and the group velocity, i.e., $|E_0^{\text{PC}}|^2/|E_0^{\text{bulk}}|^2 \propto v_g^{\text{bulk}}/v_g^{\text{PC}}$. It should be emphasized that the above derivation is valid only in the case of weak nonlinearity when the group velocity is independent of the power density of the incident wave. Otherwise, the enhancement factor will exhibit a strong dependence on the incident power density, as will be shown in Section 6.

In the case of weak nonlinearity, the group velocity $v_g$ in the PC at a certain frequency can be extracted from the enhancement factor, i.e.,

$$v_g^{\text{PC}} = \left(\frac{\sigma_{\text{bulk}}L_{\text{eff}}^{\text{bulk}}}{\sigma_{\text{PC}}L_{\text{eff}}^{\text{PC}}}\eta\right)^{-1/2} v_g^{\text{bulk}}. \tag{12}$$

Here, the group velocity in the bulk material is equal to the phase velocity when the dispersion is negligible. It implies that the $Z$-scan experiments provide an alternative way to determine the group velocity in PCs by using continuous waves instead of short pulses.

To verify the relationship between the enhancement

**Table 1. Values of $v_g$, $\sigma$, $\alpha_0$, and $L_{\text{eff}}$ for the 1D PC Used in the Calculation of $\eta$[a]**

| | $\omega(2\pi c/a)$ | | | | | | | | | |
|---|---|---|---|---|---|---|---|---|---|---|
| | *A* | *B* | *C* | *D* | *E* | *F* | *G* | *H* | *I* | *J* |
| | 0.2469 | 0.2439 | 0.2421 | 0.2353 | 0.2222 | 0.3300 | 0.3333 | 0.3367 | 0.3425 | 0.3546 |
| $v_g(c)$ | 0.268 | 0.197 | 0.244 | 0.652 | 0.354 | 0.478 | 0.197 | 0.25 | 0.697 | 0.354 |
| $\sigma$ | 0.67 | 0.62 | 0.6 | 0.58 | 0.52 | 0.12 | 0.14 | 0.16 | 0.17 | 0.2 |
| $\alpha_0$ ($\mu$m$^{-1}$) | 0.129 | 0.0012 | 0.0313 | 0.158 | 0.0004 | 0.125 | 0.0016 | 0.0865 | 0.158 | 0.0016 |
| $L_{\text{eff}}^{\text{PC}}$ ($\mu$m) | 3.686 | 4.985 | 4.628 | 3.457 | 4.995 | 3.717 | 4.98 | 4.059 | 3.454 | 4.98 |

[a]Values are derived from the linear transmission spectrum. For the bulk material ($TiO_2$ film) used as a reference, we have $T=0.985$ and $L_{\text{eff}}^{\text{bulk}}=1.985$ $\mu$m.

factor and the group velocity given in Eq. (11), we have compared the enhancement factors at different frequencies in the first and second bands derived numerically and analytically. The results are shown in Fig. 6. When using Eq. (11) to calculate $\eta$, we have employed the data for $v_g$, $\sigma$, $\alpha_0$, and $L_{\text{eff}}$ at different frequencies, which are listed in Table 1. They are derived from the linear transmission spectrum of the 1D PC. For the numerical results, we have added the results obtained at $P_{\text{in}}=50\ \text{W}/\mu\text{m}$ in order to see the effect of the incident power density on the enhancement factor.

It can be seen that in both bands the enhancement factors extracted numerically and analytically exhibit similar dependencies on frequency. However, it is noticed that a discrepancy still exists and it becomes smaller at low incident power densities. As discussed above, the group velocity will become dependent on the incident power density when the weak nonlinearity is not satisfied and it is responsible for the observed discrepancy.

## 6. POWER-DENSITY DEPENDENCE OF THE ENHANCEMENT FACTOR

The shift of photonic bands becomes obvious at high-power densities, and it may have significant impact on group velocity and enhancement factor. To find out the influence of power density on enhancement factor, we have performed numerical $Z$-scan experiments at different power densities and extracted the relationship between $\Delta T_{p-v}$ (or $\Delta\phi_0$) and $P_{\text{in}}$. The results for the bulk material ($TiO_2$ film) and the 1D PC are presented in Fig. 8. For the bulk material, a linear relationship is found and it is independent of the frequency. In contrast, a completely different relationship is observed in the 1D PC. A typical example for the relationship obtained at $\omega_B$ is given in Fig. 8. At low power densities, $\Delta T_{p-v}$ increases linearly with $P_{\text{in}}$, similar to that in the bulk material. However, the slope is much lager because of the small group velocity. With increasing $P_{\text{in}}$, the increase of $\Delta T_{p-v}$ becomes slower. After reaching a maximum value at $\sim 5\times 10^2\ \text{W}/\mu\text{m}$, $\Delta T_{p-v}$ begins to decrease with increasing $P_{\text{in}}$.

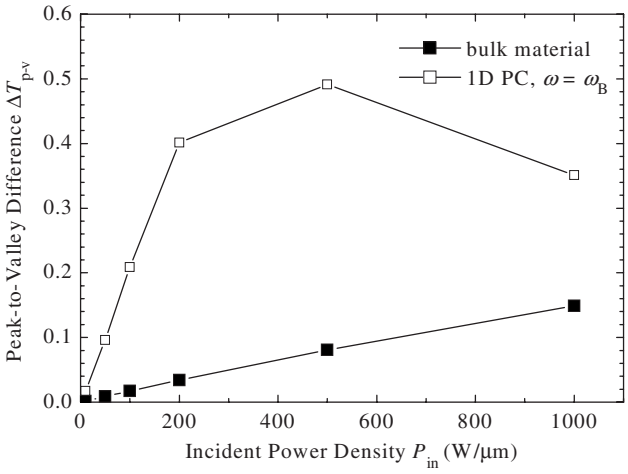


Fig. 8. (Color online) Dependence of the peak-to-valley difference in transmittance on the incident power density for the bulk material ($TiO_2$ film) and the 1D PC at $\omega_B$.

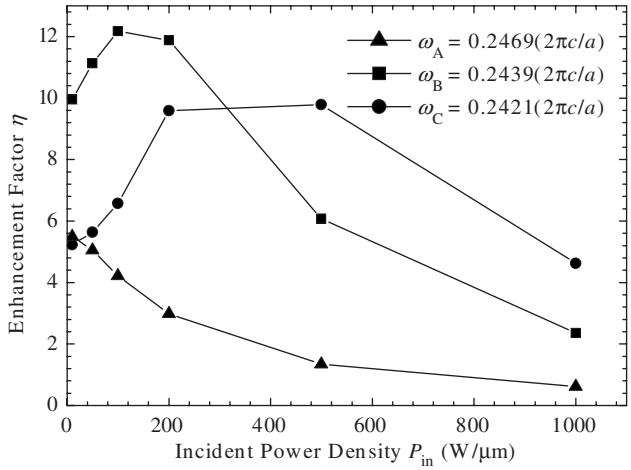


Fig. 9. (Color online) Dependence of the nonlinearity enhancement factor on the incident power density for the 1D PC at different frequencies ($\omega_A$, $\omega_B$, and $\omega_C$) in the first band.

To gain a deep insight into the dependence of the enhancement factor on the power density, we have compared the dependence of $\eta$ on $P_{\text{in}}$ for different frequencies ($\omega_A$, $\omega_B$, and $\omega_C$) in the first band, as shown in Fig. 9. Except for $\eta_A$, it is noticed that $\eta_B$ and $\eta_C$ exhibit quite similar dependences on $P_{\text{in}}$. The major difference is that the power densities at which the enhancement factors reach maximum values are different. This behavior can be interpreted by considering the variation of the group velocity with increasing power density when the shift of the photonic bands becomes effective. In Fig. 10, we have enlarged the group velocity distribution around $\omega_B$, which has been shown in Fig. 7(c). It is found that $\omega_B$ and $\omega_C$ are located on the low-frequency side of the group velocity minima while $\omega_A$ is on the high-frequency side. When the band is shifted to low frequencies, it is apparent that the group velocities at $\omega_B$ and $\omega_C$ decrease, resulting in an increase of the enhancement factor. With increasing $P_{\text{in}}$, the group velocity minimum arrives sequentially to $\omega_B$ and $\omega_C$, and $\eta_B$ and $\eta_C$ reach their maximum values. After that, the group velocity begins to increase, leading to a decrease of the enhancement factor. For $\omega_A$, a monotonic in-

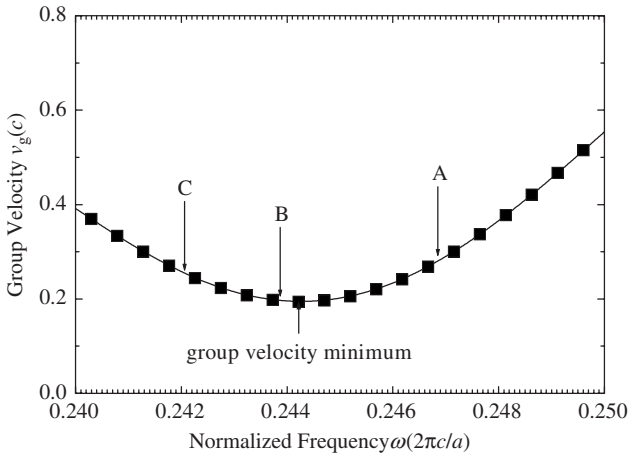


Fig. 10. (Color online) Locations of different frequencies ($\omega_A$, $\omega_B$, and $\omega_C$) in the first band relative to the group velocity minimum.

crease of the group velocity occurs when the band is shifted to a lower frequency. Correspondingly, we observe a monotonic decrease of $\eta_A$ with increasing $P_{\text{in}}$. Therefore, it is confirmed that the power-density dependence of the enhancement factor originates mainly from the power-density dependence of the group velocity. It is responsible for the discrepancy observed in Fig. 6. More importantly, it indicates that maximum enhancement can be achieved by properly choosing the frequency and the power density of the incident wave. This point is quite helpful for the design and operation of PC-based devices.

## 7. CONCLUSION

We have employed numerical *Z*-scan experiments based on the FDTD technique to investigate the nonlinearity enhancement in 1D PCs and its dependence on the incident power density. By incorporating the frequency- and power-density-dependent reflections into the linear and nonlinear absorptions of nonlinear PCs, *Z*-scan measurements and their explanations are confirmed to be applicable for nonlinear PCs. Closed and open-aperture Z-scan traces are obtained and a symmetric method is employed to modify the asymmetric closed-aperture traces. The nonlinear enhancement factors for different frequencies in the first and second bands are derived by both theoretical analysis and numerical simulation. A comparison is made between them and a good agreement is achieved. More importantly, it is revealed that the nonlinearity enhancement factor depends strongly on the incident power density and the power-density-dependent group velocity is responsible for this behavior. It suggests that the optimum performance of the devices based on nonlinear PCs can been achieved by properly choosing the working frequency and power density.

## ACKNOWLEDGMENT

The authors acknowledge financial support from the National Natural Science Foundation of China (grant 10674051), the Natural Science Foundation of Guangdong province of China (grant 06025082), and the Program for Innovative Research Team of Higher Education in Guangdong (grant 06CXTD005). S. Lan acknowledges financial support by the Program for New Century Excellent Talents (NCET) at the University of China.

## REFERENCES

1. E. Yablonovitch, "Inhibited spontaneous emission in solid-state physics and electronics," Phys. Rev. Lett. **58**, 2059–2062 (1987).
2. S. John, "Strong localization of photons in certain disordered dielectric superlattices," Phys. Rev. Lett. **58**, 2486–2489 (1987).
3. O. Painter, R. K. Lee, A. Scherer, A. Yariv, J. D. O'Brien, P. D. Dapkus, and I. Kim, "Two-dimensional photonic band-gap defect mode laser," Science **284**, 1819–1821 (1999).
4. J. S. Foresi, P. R. Villeneuve, J. Ferrera, E. R. Thoen, G. Steinmeyer, S. Fan, J. D. Joannopoulos, L. C. Kimerling, H. I. Smith, and E. P. Ippen, "Photonic crystals: putting a new twist on light," Nature **386**, 143–149 (1997).
5. S. Noda, A. Chutinan, and M. Imada, "Trapping and emission of photons by a single defect in a photonic bandgap structure," Nature **407**, 608–610 (2000).
6. M. Loncăr, D. Nedeljković, T. Doll, J. Vučković, A. Scherer, and T. P. Pearsall, "Waveguiding in planar photonic crystals," Appl. Phys. Lett. **77**, 1937–1939 (2000).
7. S. Lan, S. Nishikawa, H. Ishikawa, and O. Wada, "Design of impurity band-based photonic crystal waveguides and delay lines for ultrashort optical pulses," J. Appl. Phys. **90**, 4321–4327 (2001).
8. Y. Sugimoto, S. Lan, S. Nishikawa, N. Ikeda, H. Ishikawa, and K. Asakawa, "Design and fabrication of impurity band-based photonic crystal waveguides for optical delay lines," Appl. Phys. Lett. **81**, 1946–1948 (2002).
9. H. Kosaka, T. Kawashima, A. Tomita, M. Notomi, T. Tamamura, T. Sato, and S. Kawakami, "Superprism phenomena in photonic crystals," Phys. Rev. B **58**, R10096–R10099 (1998).
10. H. Kosaka, T. Kawashima, A. Tomita, M. Notomi, T. Tamamura, T. Sato, and S. Kawakami, "Superprism phenomena in photonic crystals: toward microscale lightwave circuits," J. Lightwave Technol. **17**, 2032–2038 (1999).
11. L. J. Wu, M. Mazilu, and T. F. Krauss, "Beam steering in planar-photonic crystals: from superprism to supercollimator," J. Lightwave Technol. **21**, 561–566 (2003).
12. M. Scalora, J. P. Dowling, C. M. Bowden, and M. J. Bloemer, "Optical limiting and switching of ultrashort pulses in nonlinear photonic band gap materials," Phys. Rev. Lett. **73**, 1368–1371 (1994).
13. H. Y. Liu, S. Lan, L. J. Wu, Q. Guo, W. Hu, S. H. Liu, X. S. Lin, and A. V. Gopal, "Self-induced Anderson localization and optical limiting in photonic crystal coupled cavity waveguides with Kerr nonlinearity," Appl. Phys. Lett. **90**, 213507 (2007).
14. P. R. Villeneuve, D. S. Abrams, S. Fan, and J. D. Joannopoulos, "Single-mode waveguide microcavity for fast optical switching," Opt. Lett. **21**, 2017–2019 (1996).
15. S. Lan, A. V. Gopal, K. Kanamoto, and H. Ishikawa, "Ultrafast response of photonic crystal atoms with Kerr nonlinearity to ultrashort optical pulses," Appl. Phys. Lett. **84**, 5124–5126 (2004).
16. Y. H. Liu, X. Y. Hu, D. X. Zhang, B. Y. Cheng, D. Z. Zhang, and Q. B. Meng, "Subpicosecond optical switching in polystyrene opal," Appl. Phys. Lett. **86**, 151102 (2005).
17. A. Haché and M. Bourgeois, "Ultrafast all-optical switching in a silicon-based photonic crystal," Appl. Phys. Lett. **77**, 4089–4091 (2000).
18. X. Y. Hu, Q. Zhang, Y. H. Liu, B. Y. Cheng, and D. Z. Zhang, "Ultrafast three-dimensional tunable photonic crystal," Appl. Phys. Lett. **83**, 2518–2520 (2003).
19. N. S. Zhao, H. Zhou, Q. Guo, W. Hu, X. B. Yang, S. Lan, and X. S. Lin, "Design of highly efficient optical diodes based on the dynamics of nonlinear photonic crystal molecules," J. Opt. Soc. Am. B **23**, 2434–2440 (2006).
20. M. Soljačić, S. G. Johnson, S. Fan, M. Ibanescu, E. Ippen, and J. D. Joannopoulos, "Photonic-crystal slow-light enhancement of nonlinear phase sensitivity," J. Opt. Soc. Am. B **19**, 2052–2059 (2002).
21. J. Hwang, N. Y. Ha, H. J. Chang, B. Park, and J. W. Wu, "Enhanced optical nonlinearity near the photonic bandgap edges of a cholesteric liquid crystal," Opt. Lett. **29**, 2644–2646 (2004).
22. J. Hwang and J. W. Wu, "Determination of optical Kerr nonlinearity of a photonic bandgap structure by *Z*-scan measurement," Opt. Lett. **30**, 875–877 (2005).
23. M. Sheik-Bahae, A. A. Said, T. Wei, D. J. Hagan, and E. W. Van Stryland, "Sensitive measurement of optical nonlinearities using a single beam," IEEE J. Quantum Electron. **26**, 760–769 (1990).
24. J. Hwang and J. W. Wu, "Investigation on dispersive properties of photonic crystals for employment of *Z*-scan method," Proc. SPIE **6480**, 648019 (2007).
25. K. Yee, "Numerical solution of initial boundary value problems involving Maxwell's equations in isotropic

media," IEEE Trans. Antennas Propag. **14**, 302–307 (1966). In this paper, a commercial software developed by Rsoft Design Group (http://www.rsoftdesign.com) is used for FDTD simulations.
26. J. Hwang, M. J. Kim, J. W. Wu, S. M. Lee, and B. K. Rhee, "Picosecond pump-probe measurement of bandgap changes in $SiO_2/TiO_2$ one-dimensional photonic bandgap structures," Opt. Lett. **31**, 377–379 (2006).
27. Z. B. Liu, J. G. Tian, W. P. Zang, W. Y. Zhou, C. P. Zhang, and G. Y. Zhang, "Influence of nonlinear absorption on *Z*-scan measurements of nonlinear refraction," Chin. Phys. Lett. **20**, 509–512 (2003).
28. N. C. Panoiu, M. Bahl, and R. M. Osgood, Jr., "Ultrafast optical tuning of a superprism effect in nonlinear photonic crystals," J. Opt. Soc. Am. B **21**, 1500–1508 (2004).